

Echoes of Galactic Supernovae

Armin Rest (Harvard University) & Chris Smith (NOAO)
for the Echoes of Historical Supernovae (EHS) Team

Light echoes from ancient supernovae offer a unique and powerful opportunity to study supernovae and their relationships to supernova remnants (SNRs), as well as interstellar dust and Galactic structure. The use of this relatively simple phenomenon of light echoes in such studies is just now developing into an exciting new field of study. This is one of the very rare occasions in astronomy that the cause and effect of the same astronomical event can be observed, in that we can study the physics of the SNR as it appears now and also the physics of the explosion that produced it hundreds of years ago.

We define a light echo as reflected light from a light source, not reprocessed light. Similar to the muffled echo of sound when someone shouts something toward a wall, the light echo still contains the initial signature of the original light, even if the precise signature is somewhat modified by details of the reflecting surface. Since the reflected light traverses a longer path than the light that takes the direct path to the observer, it will be observed some time after the initial explosion is observed.

Our group pioneered the optical discovery and study of ancient supernova light echoes in the LMC, where three echo complexes were found to be associated with 400-900 year-old supernova remnants (Rest et al., 2005b). The spectra of one of those echoes (Rest et al., 2008a) allowed us to classify the event as a specific subtype of the Type Ia, which in this case was from an overluminous SN Ia. This was the first time that the type of a SN could be unambiguously determined based on the spectrum of maximum light of the supernova centuries after the light on the direct path had reached Earth.

Echo features similar to those we discovered in the LMC should be detectable within our own Milky Way—the challenge is to locate them across a much larger solid angle. For example, the angular distance between a light echo of a Galactic SN at a distance of 3,000 pc

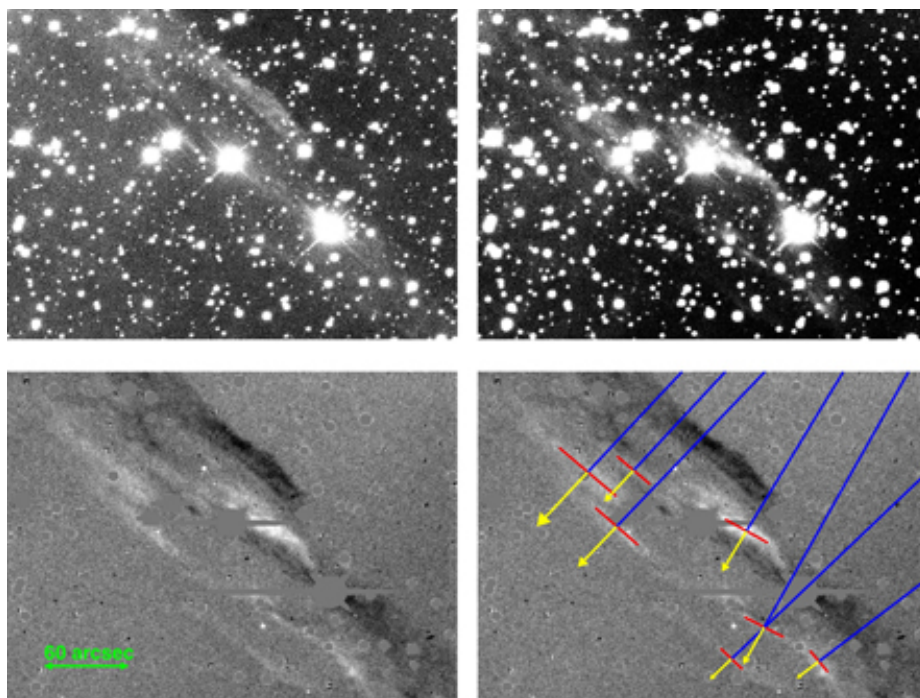


Figure 1

to the SNR may be tens of times larger than if the same SN and reflecting dust were located in the LMC. Thus the search annuli for light echoes of Galactic SNe can have an outer radius up to 20 degrees.

We have undertaken a program using the CTIO and KPNO 4-meter telescopes with the NOAO Mosaic imagers to find echoes around the seven certain historical Galactic SNe recorded in the last 2,000 years (Stephenson & Green, 2002): SN 185 AD/Centaurs, SN 1054 AD/Crab, SN1006 AD/Lupus, SN 1181 AD/Cassiopeia, Tycho, Kepler, and Cas A. Given the relatively well-constrained ages of these historical supernovae and estimated distances, we can improve our chance to find echoes by targeting regions of cold dust at the approximate expected angular distance. We used the reprocessed 100-micron IRAS images (Miville-Dechenes & Lagache, 2005) to select fields with lines of sight which contain such dust, choosing fields closer to

the Galactic plane than the supernovae in the expectation that dust would be more highly concentrated there. Two epochs of imaging data were kernel- and flux-matched, aligned, subtracted, and masked using the techniques developed for the LMC echo searches (Rest et al., 2005a).

Careful visual inspection of our clean difference images revealed many candidate echo arclets, such as those shown in figure 1. We estimated the individual arc-motion directions as shown in the figure, and grouped the clusters of arclets into echo complexes. To date, we have discovered two distinct echo complexes (panel A of figure 2). One complex consists of six clusters of light echoes with proper motion vectors converging back to the Cas A SNR, and the other complex is composed of six echo clusters with an origin coincident with the Tycho SNR (Rest et al., 2008b). Panel B shows the average vector for each light echo cluster. Krause et al. (2008)

continued

Echoes of Galactic Supernovae continued

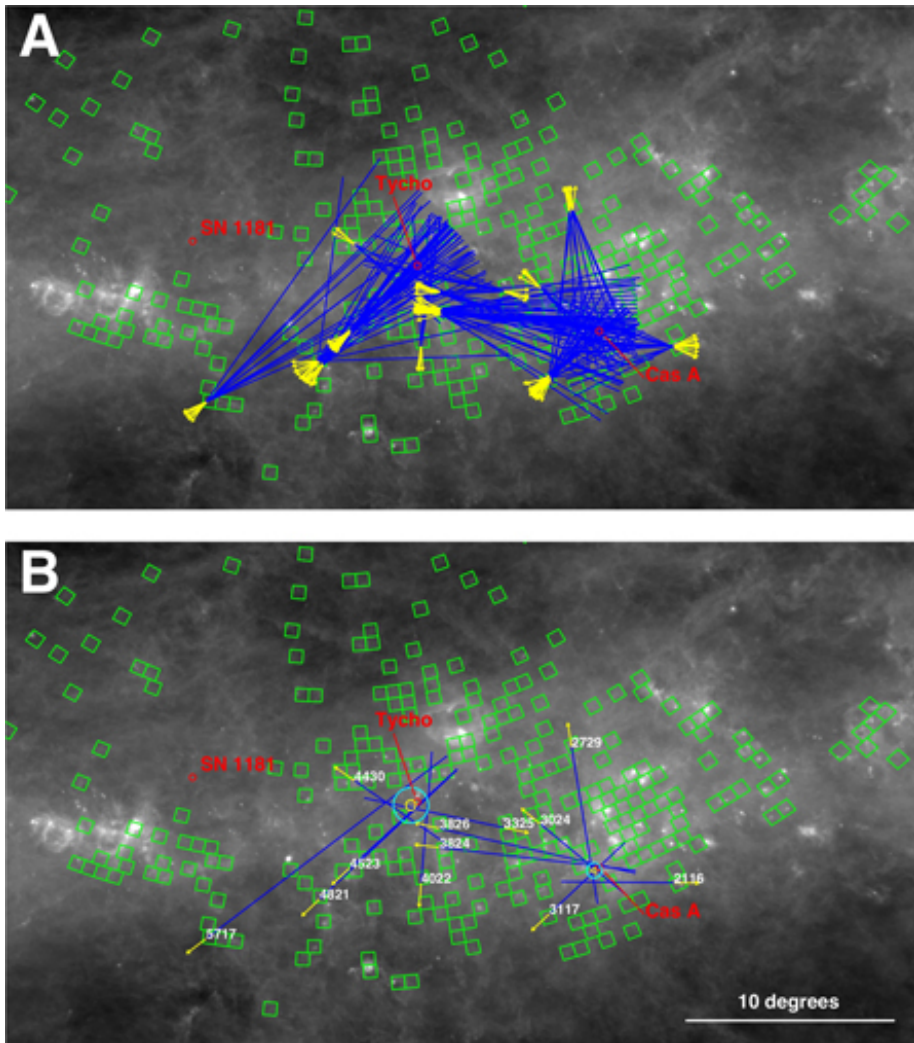


Figure 2

have also discovered an apparent light echo from Cas A at a much smaller apparent angular distance from the remnant.

These scattered-light echoes from Galactic SNe provide a host of newly-recognized observational benefits:

- **SN type classification:** For Cas A, Krause et al. (2008) have obtained a spectrum of the echo they discovered, which indicates a classification of Type IIb for the SN. We hope to obtain spectroscopy of several more Cas A echoes to obtain confirmation.


For Tycho, we hope to determine the SN Ia subtype with our follow-up spectroscopy.

- **Distance to the SNR:** The *geometric* distance to the source of light echoes can be determined to high accuracy with polarization measurements of its light echoes (Sparks, 2008). This method works best for light echoes with a scattering angle spread around 90 degrees, which corresponds to a distance spread around $z=0$, where z is the distance from the supernova to the scattering dust projected along our line of sight. This is the case for the echoes we have

discovered from Tycho. For Cas A we need several more light echo groups closer to the SNR. The existence of re-radiated echo light in the infrared (Krause, 2005) suggests that further scattered-light echoes closer to Cas A should be detectable.

- **Asymmetry of SN explosion:** Light echoes offer another rare occasion in astronomy, in that the spectra of echo arcs at different position angles is equivalent to different hemispheres of the photosphere. Tycho is a perfect candidate for this study: we will be able to look at Tycho from *opposite* sides due to the favorable locations of the scattering dust! Testing the asymmetry of SN Ia is very important for our understanding of the physics of these explosions, especially given that Type Ia SNe are used as cosmological standard candles.

Beyond these supernova-related benefits, complexes of light echoes can help us map out and understand the structure of dust sheets in the Galaxy, and possibly understand the characteristics of the dust itself. With further observations of the regions around historical supernovae, we hope to find more examples of these exciting “ghosts,” which move through the sky with apparent motions of 20 to 40 arcsec per year.

Note: The discovery paper of the Cas A and Tycho echoes was dedicated to Howard Lanning, a valuable member of the “Echoes of Historical Supernovae” team who passed away on 20 December 2007. 

REFERENCES

Krause, O., et al. 2008, *Science*, in press
 Krause, O., et al. 2005, *Science*, 308,1604
 Miville-Deschenes, M.-A. & Lagache, G. 2005, *ApJS*, 157, 302
 Rest, A., et al. 2005a, *ApJ*, 634, 1103
 Rest, A., et al. 2005b, *Nature*, 438, 1132
 Rest, A., et al. 2008a, *ApJ*, 680, 1137
 Rest, A., et al. 2008b, *ApJL*, 681, 81
 Stephenson, F. R., & Green, D. A. 2002, *Historical Supernovae and Their Remnants*, International Series in Astronomy and Astrophysics, vol 5. Oxford: Clarendon Press, 2002, ISBN 0198507666
 Sparks, W. B., et al 2008, *AJ*, 135, 605

Observations of a Small Emergent Bipolar Flux Region

Alexandra Tritschler (NSO), Kevin Reardon & Gianna Cauzzi (Arcetri Observatory)

The Sun has not been very active lately, with only a handful of active regions appearing on the disk in many months. For this reason, we are excited about being able to capture the emergence phase of a small, old-cycle, bipolar region close to disk center on 22 April 2008. During almost four hours of exceptionally good seeing conditions, the Interferometric Bidimensional Spectrometer (IBIS) scanned repeatedly through four spectral lines (Fe I 709.04 nm, Na I 589.6 nm, H I 656.3 nm, Ca II 854.21 nm), covering the height range from the photosphere to the chromosphere. The narrowband observations are supported by simultaneous broadband observations at 721 nm and in the G Band around 430.5 nm. The small bipolar region was not visible in the late afternoon on the previous day, and decayed completely during the two days following our observations.

Although IBIS was operated in a non-polarimetric mode, these observations are of particular interest and importance for two reasons. First, we witnessed the transformation of filamentary structures (a rudimentary penumbra) into a small but fully developed penumbral segment in the photospheric layers of one of the formerly naked umbrae, in concert with the formation of a small light bridge. The evolution of active regions has been extensively studied for decades, and much progress has been achieved in understanding how flux is transported from deep in the convection zone to emerge at the solar surface in the form of sunspots. However, we still do not have a comprehensive picture of the detailed process of penumbral formation and decay, because observations of this precious moment in time are extremely rare.

Figure 1 shows the 75×75 arcsec field of view (FOV) of IBIS (left) and depicts some moments during the transformation process based on speckle-reconstructed broad-band observations (right, from a to d in time, 26×26 arcsec FOV). Interestingly, the penumbral segment was formed on the side of the pore that faces the opposite polarity (parallel to the line which connects the two parts of the bipolar region, about two o'clock in the figure).

Second, the chromospheric observations give strong evidence for large redshifts in both legs of the loop(s) that connect the two pores. Prelimi-

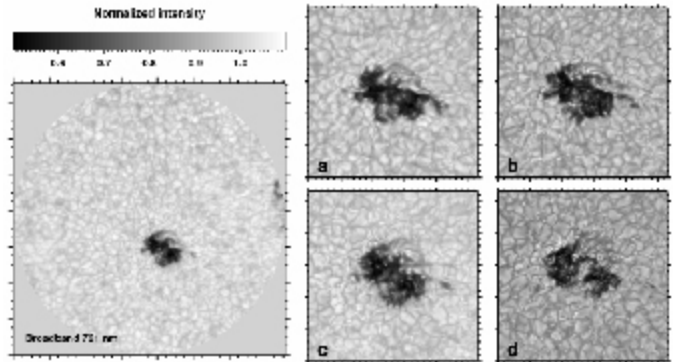


Figure 1: Left panel shows normalized broadband intensity at 721 nm (in units of the mean quiet Sun) showing the 75×75 arcsec FOV observed with IBIS. Right panel shows individual speckle reconstructions showing four different time steps during the transformation process of a rudimentary penumbra into a penumbral segment.

nary line-of-sight (LOS) velocities confirmed this impression, indicating line-core Doppler shifts that correspond to velocities in the range of 10-20 km/s (see figure 2; the velocities in the Ca II Dopplergram have been clipped for better visibility of the fine structure in the flow field). Inspecting the Ca II 854.21 nm line profiles directly, we note the presence of strong line asymmetries in the form of redshifted line satellites.

In between the two redshifted legs we see indication of a blueshift. Considering the closeness to disk center, we interpret the measured LOS velocities as real upflows and downflows and speculate that we have captured the drainage of the rising magnetic loop associated with the bipolar region. Supersonic chromospheric downflows have been detected before, particularly in the footpoints of arch filament systems from H α observations (e.g., Bruzek, *Solar Physics*, 1969), but the combination of spectral and temporal coverage and excellent spatial resolution makes our observations very unique.

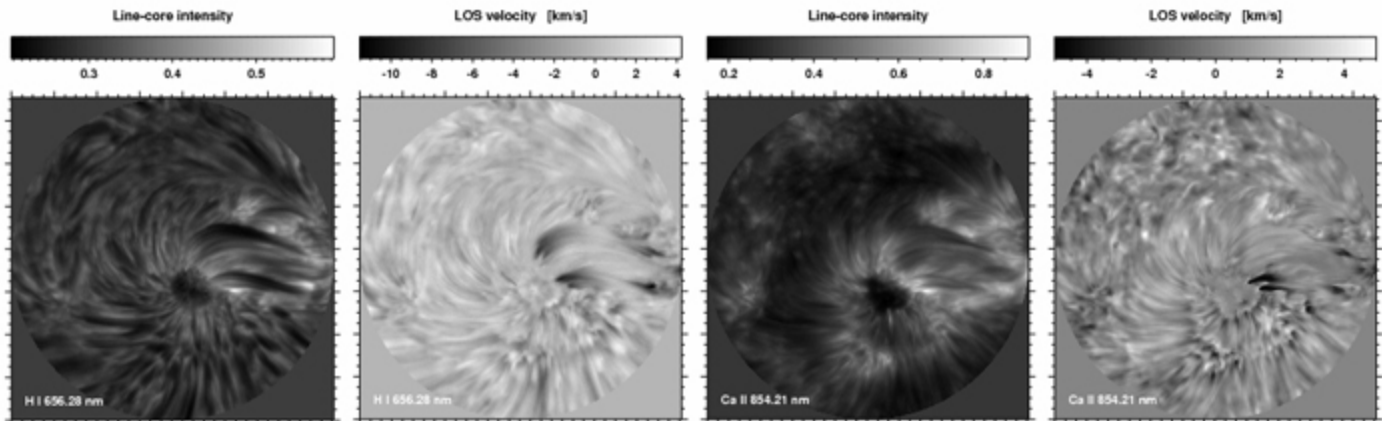


Figure 2. From left to right, line-core intensity and line-of-sight Dopplergram of H α and the Ca II 854.21 nm line, respectively. The FOV corresponds to 75×75 arcsec.

Carbon-enhanced Metal-poor Stars and the Chemical Evolution of the Early Galaxy

Simon Schuler

Very metal-poor stars ($[Fe/H] \leq -2.0$) are relics of the earliest stellar populations, and the chemical abundances of their photospheres are signatures of the nucleosynthetic processes that occurred in the young Milky Way. Mapping the abundance patterns of these very metal-poor (VMP) stars provides stringent constraints for stellar nucleosynthesis and Galactic chemical evolution models.

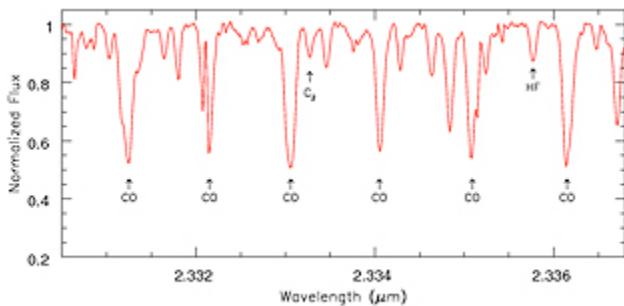


Figure 1: High-resolution near-IR Phoenix spectrum of the CEMP star HE 1305+0132 obtained with Gemini South. The spectrum is characterized by a resolution of $R = 50,000$ and a per pixel signal-to-noise of 129. The HF (1-0) R9 line can be seen at 2.3358 microns. The prominent $^{12}C^{16}O$ lines in the region are marked, as is a lone feature of the Phillips C₂ system.

The number of identified VMP stars in the Galactic halo has increased significantly over the past decade or so, thanks to objective prism surveys such as the HK (Beers, Preston, & Shectman 1985, 1992) and Hamburg/ESO (HES; Wisotzki et al. 2000; Christlieb 2003) projects, and more recently, the Sloan Extension for Galactic Understanding and Exploration (SEGUE), a component of the first extension of the Sloan Digital Sky Survey (SDSS). Follow-up medium resolution spectroscopy—or in the case of SEGUE, the SDSS medium spectra themselves—have revealed that somewhere between 10-25% of VMP stars show surprisingly large enhancements of carbon ($[C/Fe] \geq +1.0$). The fraction increases at lower metallicities, reaching 40% of stars at $[Fe/H] \leq -3.5$ and 100% at $[Fe/H] \leq -4.0$, of which only three are currently known (e.g., Norris et al. 2007). The increased incidence of these so-called carbon-enhanced metal-poor (CEMP) stars at ever-decreasing metallicities suggests that the nucleosynthetic pathways leading to these interesting objects were highly efficient in the early Galaxy and that they played an important role in Galactic chemical evolution.

In addition to carbon, about 75% of CEMP stars are also enhanced in barium ($[Ba/Fe] \geq +0.50$), a heavy element that is produced by the slow-neutron capture process (s-process) in the He-burning shells of thermally pulsating asymptotic giant branch (AGB) stars. Many of these stars, known as CEMP-s stars, do not have visible companions, but they have been identified through radial velocity measurements to be members of binary systems. Together, the s-process element enhancement and the binarity strongly suggest that CEMP-s stars have been contaminated by an evolved companion as it passed through its AGB phase.

Carbon, nitrogen, oxygen, and s-process element abundances derived from high-resolution spectra of CEMP-s stars provide important constraints for models of metal-poor AGB star nucleosynthesis. Stronger constraints can be applied to the models, however, by considering the abundance of an additional element, ^{19}F .

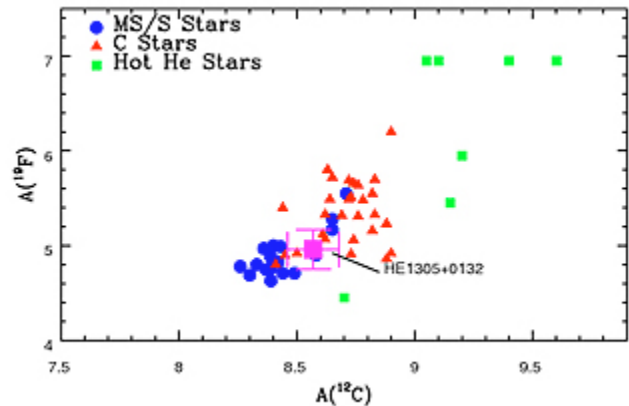


Figure 2: Logarithmic abundances of ^{19}F plotted against those of ^{12}C . The abundances of HE 1305+0132 are given by the large square with error bars and fall right on the trend defined by stars known to have been contaminated by AGB star companions. This figure is adapted from Schuler et al. (2007).

^{19}F is the only stable isotope of fluorine, and one of its production sites is also the He-burning shell of an AGB star. The reaction chain responsible is $^{14}N(\alpha, \gamma) ^{18}F(\beta^+) ^{8}O(\text{proton}, \alpha) ^{15}N(\alpha, \gamma) ^{19}F$. The protons captured by ^{18}O are provided by the $^{14}N(\text{neutron}, \text{proton}) ^{14}C$ reaction, for which the required neutrons are provided by the $^{13}C(\alpha, \text{neutron}) ^{16}O$ reaction. ^{13}C and ^{14}N are produced in the surrounding H-burning shell and subsequently mixed down into the He shell.

Our group is conducting an observational program using the high-resolution ($R = \lambda/\Delta\lambda = 50,000$) near-IR Phoenix spectrograph on the Gemini South 8-meter telescope to derive ^{19}F of CEMP stars. ^{19}F abundances of late-type stars can only be derived from near-IR K-band spectral features arising from vibration-rotation transitions of the hydrogen fluoride (HF) molecule. For our program, we have specifically targeted the (1-0) R9 line at 2.3358 microns (see figure 1).

One of the first CEMP stars we observed, HE 1305+0132, showed a strong HF feature in its Phoenix spectrum that suggested a highly enhanced ^{19}F abundance. Indeed, our abundance analysis revealed that it has a ^{19}F abundance ($A(^{19}F) = 4.96 \pm 0.21$ or $[F/Fe] = 2.90$) that is almost three orders of magnitude greater than that of the Sun (Schuler et al., 2007)!

Figure 2 places the enhanced ^{19}F abundance of HE 1305+0132 into context. In the figure, the $A(^{19}F)$ abundances of three classes of stars are plotted against their $A(^{12}C)$ abundances. The MS/S stars

continued


Carbon-enhanced Metal-poor Stars continued

are intrinsic thermally pulsating AGB stars, the C stars are stars known to have been polluted by an AGB companion, and the hot He stars are essentially the exposed cores of former AGB stars. The abundances of HE 1305+0132 fall right on the A(19F)-A(12C) trend defined by the MS/S/C stars, pointing to an AGB nucleosynthesis origin of its 12C and 19F.

At the time of our analysis, no high-resolution abundance analysis had been carried out for HE 1305+0132, so it was not known beforehand if it fell into the CEMP-s star category, as the 19F abundance suggests. Our group has since obtained a high-resolution optical spectrum of this star using the High-Resolution Spectrograph (HRS) on the 9.2-meter effective aperture Hobby-Eberly Telescope (HET) with time granted through NOAO and the Telescope System Instrumentation Program (TSIP). Analysis of the HET/HRS spectrum is ongoing, but preliminary results suggest that the Ba abundance of HE 1305+0132 is near $[Ba/Fe] = +1.0$, solidly placing it in the CEMP-s category.

With Gemini South/Phoenix spectra of an additional 10 CEMP stars obtained in the 2007A and 2007B semesters, our analysis of 19F in CEMP stars continues. We have also recently been granted for this project 10.1 hours of time on the 8.2-meter ANTU (unit 1) telescope of the Very Large Telescope to use the new high-resolution near-IR

spectrograph CRIRES; our target list includes seven more CEMP stars. With the successful completion of the CRIRES program, our total sample will include 17 CEMP stars for which we will derive 19F abundances. These data will allow us to further constrain low-metallicity AGB star nucleosynthesis and the chemical histories of CEMP stars. Making progress in both of these areas will greatly improve our understanding of early Galactic chemical evolution.

I gratefully acknowledge my collaborators involved with this project: Katia Cunha and Verne V. Smith at NOAO, and Thirupathi Sivarani, Timothy C. Beers, and Young Sun Lee at Michigan State University/Joint Institute for Nuclear Astrophysics. 

REFERENCES

- Beers T., Preston R., & Shectman, S. 1985, *AJ*, 90, 2089
 Beers, T., Preston R., & Shectman, S. 1992, *AJ*, 103, 1987
 Christlieb, N. 2003, *The Cosmic Circuit of Matter*, ed. R. Scheilicke (Wiley), 191
 Norris, J. et al., 2007, *ApJ*, 670, 774
 Schuler, S., Cunha, K., Smith, V., Sivarani, T., Beers, T., and Lee, Y. S. 2007, *ApJ*, 667, L81
 Wisotzki, L., Christlieb, N., Bade, N., Beckmann, V., Koehler, T., Vanelle, C., & Reimers, D., 2000, *A&A*, 358, 77

Do Solar Subsurface Vorticity Measurements Improve Flare Forecasting?

Rudi Komm, Frank Hill (NSO) & Ryan Ferguson (REU/Michigan State University)

Regions of strong magnetic fields (active regions) are the locations of strong eruptive phenomena such as flares and coronal mass ejections, which can disrupt technology on Earth. Highly twisted magnetic fields are very probably responsible for these phenomena. These fields extend from below the surface through the solar atmosphere into the interplanetary medium (heliosphere). Flows below the solar surface are accessible with the techniques of local helioseismology, which are currently the only way to measure anything related to active regions below the solar surface.

Subsurface flows below active regions are rather complex (see figure 1, next page). Besides showing in- or outflows varying with depth, the subsurface flows below active regions are highly twisted (Komm, 2007). This twist can be measured by the vorticity vector (curl of velocity) which corresponds to changing orientation in space of fluid, and is thus a quantity associated with mixing. The zonal (east-west) and the meridional (north-south) component of the vorticity vector show a dipolar pattern of opposite signed values below strong active regions (see figure 1).

This pattern is analogous to two smoke rings stacked on top of each other and coincides with locations of flare activity in active regions. In a previous study (Mason et al., 2006), we defined a quantity to capture this pattern in a single value and found that flare activity is in-

trinsically linked to subsurface phenomena on timescales and spatial scales comparable to the lifetime and size of active regions. The question remains whether the measured vorticity of subsurface flows can help to improve the forecasting of flare activity of active regions.

We have begun to address this question using the data set from the previous study, which Ryan Ferguson (a NSO 2008 Research Experiences for Undergraduates student from Michigan State University) extended to include data through 2007. The data set is the largest of its kind and consists of 1,009 active regions and their subsurface flow measurements derived from Global Oscillation Network Group (GONG) data. The data set also includes the magnetic flux of each active region from NSO/Kitt Peak and Synoptic Optical Long-term Investigations of the Sun synoptic maps, and the corresponding X-ray flare information from the Geostationary Operational Environmental Satellite (GOES). We determine solar subsurface flows with a ring-diagram analysis and remove the average differential rotation and the average meridional flow to focus on the variation of the flows associated with active regions.

Some of the results are presented here. The left panel of figure 2 shows the total flare intensity of active regions, which is a proxy of their total X-ray flare activity over an active region's lifetime. A flare-prolific active region is clearly characterized by large magnetic flux

continued

Do Solar Subsurface Vorticity Measurements Improve Flare Forecasting? continued

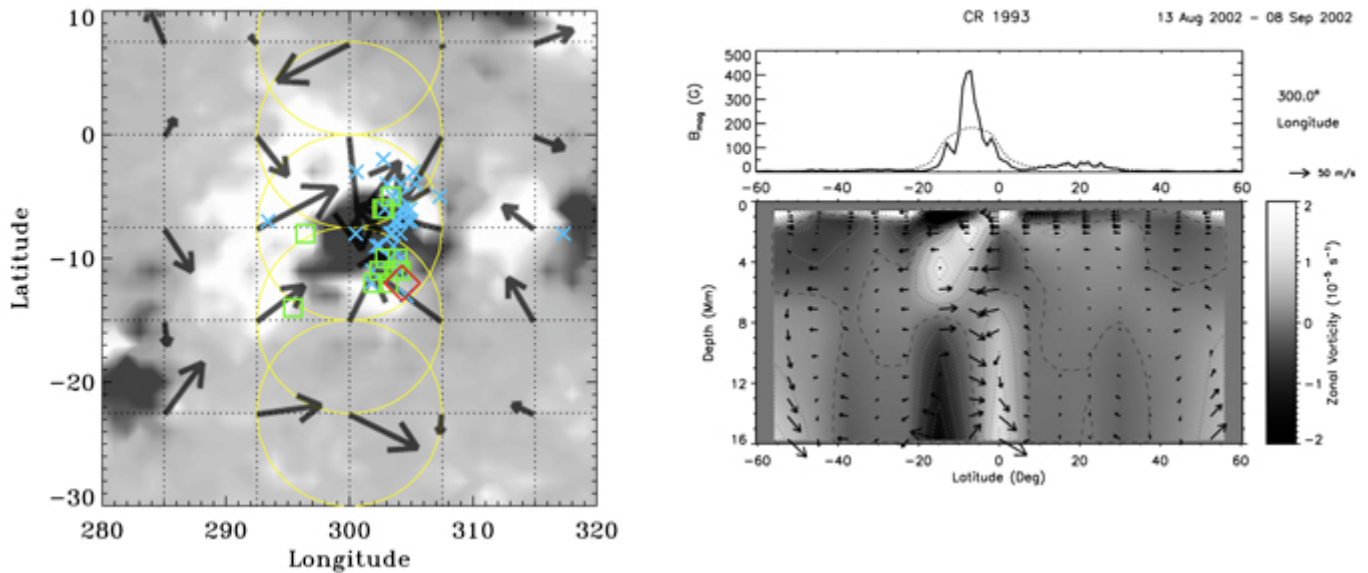



Figure 1: The left panel shows the surface magnetic field of active region 10,069. Flare locations are superposed with cross symbols for C-class flares, squares for M-class flares, and a diamond symbol for an X-class flare. The subsurface velocities at a depth of 7 Mm are superposed as arrows corresponding to values of about 30 m s^{-1} . Open circles indicate dense-pack patches at 300° longitude. All flares are located within the dense-pack patch located at -7.5° latitude and 300° longitude. The right panel shows a grey-scale slice of the zonal vorticity component at the same longitude with meridional flows superposed as arrows and a line drawing of the unsigned magnetic flux on top. The location of active region 10,069 coincides with large vorticity values; the flows below the active region are highly twisted. The dipolar vorticity pattern is typical of strong active regions that produce many flares.

and large vorticity values. A large magnetic flux is not sufficient to determine whether a given active region will be flare-prolific or not. Even at high flux values, there are active regions with low vorticity that do not produce energetic flares. The middle panel shows the same for the M-class of X-ray flares. (Of the 1,009 active regions analyzed, 425 regions produced at least a C-class flare, while 130 regions produced at least an M-class flare and only 19 regions produced an X-class flare.) It is clear that the strongest flares occur when both the flux and the vorticity values are high.

From this result, we can deduce the probability that an active region within a certain range of vorticity and magnetic flux produces an M-class flare, as shown in the right panel. This probability is 81% for

a region in the bin with the largest flux and vorticity values compared to an overall probability of 44% for the four bins with the largest magnetic flux or only 13% for the whole data set. It is clearly beneficial to include the vorticity information in this case. We find similar results for C- and X-class flares.

The inclusion of subsurface vorticity improves the ability to distinguish between flaring and non-flaring active regions compared to using magnetic flux alone. The results presented here characterize the average behavior of active regions during their disk passage and not their evolution on much shorter time scales. We expect to present results on the temporal variation of subsurface flows of active regions related to their flare activity in the near future. 

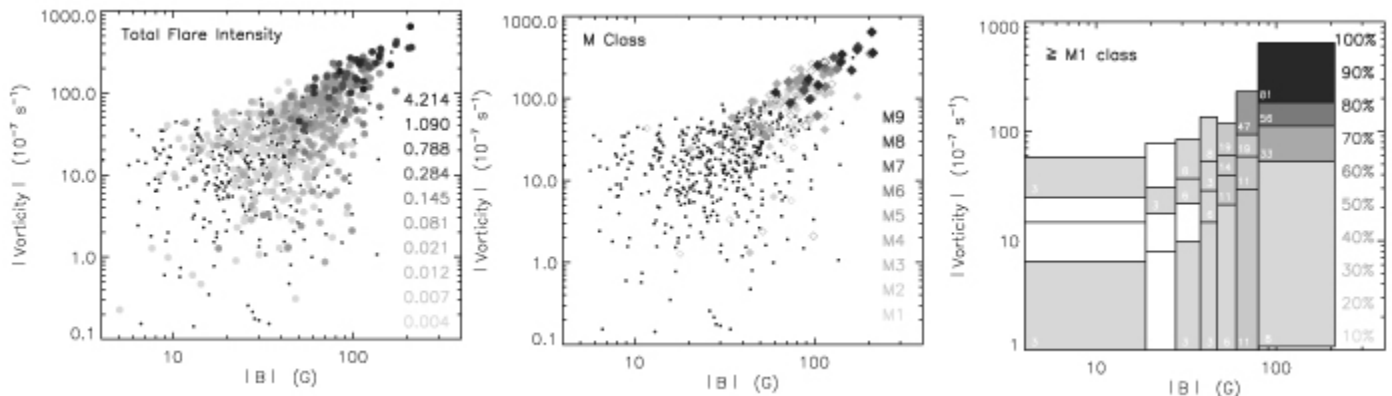


Figure 2: The left panel shows the surface magnetic field B and vorticity of 1,009 active regions. Grey circles indicate the flare intensity levels summed over all flares in each region. (Black crosses indicate non-flaring active regions). The flares occur mainly when the active regions have high values of both B and vorticity. The middle panel shows a similar plot but for M-class flares only. Filled (open) diamond symbols indicate active regions that produced multiple (only one) M-class flares. The right panel divides up the active regions so that each box contains an equal number of points. The number in the bins are the percentage of active regions with at least one flare with an M-class or greater magnitude. Grey scales indicate the probability levels in steps of 10%, white is zero. It is clear that the strongest flares occur when both B and vorticity are high.